FZD-487

Turbulent Dispersion of Bubbles in Poly-dispersed Gas-Liquid Flows in a Vertical Pipe

and

Validation of the Multiple Velocity Multiple Size Group (CFX10.0 N x M MUSIG) Model for Polydispersed Multiphase Flows

Jun-Mei Shi, Ulrich Rohde, Horst-Michael Prasser

September 2007

Wissenschaftlich-Technische Berichte
FZD-487 2007 · ISSN 1437-322X

WISSENSCHAFTLICH-TECHNISCHE BERICHTE

Forschungszentrum Dresden Rossendorf

Wissenschaftlich-Technische Berichte
FZD-487
September 2007

Jun-Mei Shi, Ulrich Rohde, Horst-Michael Prasser

Turbulent Dispersion of Bubbles in Poly-dispersed Gas-Liquid Flows in a Vertical Pipe

Technical Report

Forschungszentrum Dresden Rossendorf

Jun-Mei Shi, Ulrich Rohde, Horst-Michael Prasser

Turbulent Dispersion of Bubbles in Poly-dispersed Gas-Liquid Flows in a Vertical Pipe

Technischer Fachbericht
Turbulente Blasendispersion in einer polydispersen Rohrströmung

Technical Report
Turbulent Dispersion of Bubbles in Poly-dispersed Gas-Liquid Flows in a Vertical Pipe

Reaktorsicherheitsforschung-Vorhaben-Nr./ Reactor Safety Research-project No.: 150 1265

Vorhabenstitel: **Aufbau und Durchführung von Experimenten an der Mehrzweck-Thermohydraulikversuchsanlage TOPFLOW für generische Untersuchungen von Zweiphasenströmungen und die Weiterentwicklung und Validierung von CFD-Codes.**

Project Title: **Construction and execution of experiments at the multi-purpose thermal hydraulic test facility TOPFLOW for generic investigations of two-phase flows and the development and validation of CFD codes.**

Autoren / Author(s): **Jun-Mei Shi, Ulrich Rohde, Horst-Michael Prasser**

Dienststelle der Autoren / Performing Organisation: **Forschungszentrum Dresden-Rossendorf e.V. Institut für Sicherheitsforschung**

Berichtsdatum / Publication Date: **September 2007**

Berichts-Nr. / Report-No.: **FZD-487**

Das diesem Bericht zugrunde liegende Vorhaben wurde mit Mitteln des Bundesministeriums für Wirtschaft und Technologie unter dem Förderkennzeichen 150 1265 gefördert. Die Verantwortung für den Inhalt dieser Veröffentlichung liegt bei den Autoren.

Berichtsblatt

1. ISBN oder ISSN	2. Berichtsart Technischer Fachbericht
3a. Titel des Berichts Turbulente Blasendispersion in einer polydispersen Rohrströmung	
3b. Titel der Publikation	
4a. Autoren des Berichts (Name, Vorname(n)) Jun-Mei Shi, Ulrich Rohde, Horst-Michael Prasser	5. Abschlussdatum des Vorhabens 30.09.2006
	6. Veröffentlichungsdatum September 2007
4b. Autoren der Publikation (Name, Vorname(n))	7. Form der Publikation Broschüre
8. Durchführende Institution(en) (Name, Adresse) Forschungszentrum Dresden-Rossendorf e.V. Institut für Sicherheitsforschung Postfach 510119 01314 Dresden	9. Ber.Nr. Durchführende Institution
	10. Förderkennzeichen *) 150 1265
	11a. Seitenzahl Bericht
	11b. Seitenzahl Publikation
13. Fördernde Institution (Name, Adresse) Bundesministeriums für Wirtschaft und Technologie (BMWi) 11019 Berlin	12. Literaturangaben 17
	14. Tabellen 1
	15. Abbildungen 6
16. Zusätzliche Angaben	
17. Vorgelegt bei (Titel, Ort, Datum)	

18. Kurzreferat

Die turbulente Dispersion ist ein wichtiges Phänomen in Mehrphasenströmungen. Sie hat starken Einfluss auf die lokale Verteilung der dispersen Phase. Die physikalische Ursache der turbulenten Dispersion liegt in der Wechselwirkung der einzelnen Partikel der dispersen Phase mit den Turbulenzwirbeln der kontinuierlichen Phase. In einer Lagrange'schen Betrachtungsweise kann ein entsprechendes Modell für die Wechselwirkung eingebaut und separat für jedes Partikel berücksichtigt werden. Dafür ist allerdings eine sehr hohe Orts- und Zeitauflösung erforderlich, die solche Simulationen auf kleinskalige Probleme mit wenigen dispersen Partikeln beschränkt. Daher wird für Strömungen mit höherer Partikelbeladung i.a. eine Eulerscher Betrachtungsweise benutzt. In diesem Fall wird die turbulente Dispersion in Form eines turbulenten Diffusionsterms in der Massenerhaltungsgleichung und einer turbulenten Dispersionskraft in der Impulserhaltungsgleichung berücksichtigt. Der Diffusionsterm verschwindet im Fall einer Favre-Mittellung (massengewichtete Mittelung) der Geschwindigkeit in den Transportgleichungen. Die turbulente Dispersionskraft ergibt sich hingegen aus dem Turbulenzeffekt der Kräfte an den Phasengrenzflächen. Oft ist dabei nur der Schwankungsanteil der der Drag-Kraft wichtig. Daher berücksichtigen viele der in der Literatur verfügbaren Modelle nur diesen Anteil. Im vorliegenden Bericht wird eine neue und allgemeinere Form der turbulenten Dispersionskraft abgeleitet und validiert.

19. Schlagwörter

Blasenströmung, Impulsaustausch, Blasenkräfte, Turbulente Dispersionskraft, Favre Mittelung

20. Verlag	21. Preis

Document Control Sheet

1. ISBN or ISSN	2. Type of Report Technical Report
3a. Report Title Turbulent Dispersion of Bubbles in Poly-dispersed Gas-Liquid Flows in a Vertical Pipe	
3b. Title of Publication	
4a. Author(s) of the Report (Family Name, First Name(s)) Jun-Mei Shi, Ulrich Rohde, Horst-Michael Prasser	5. End of Project 30.09.2006
	6. Publication Date September 2007
4b. Author(s) of the Publication (Family Name, First Name(s))	7. Form of Publication Booklet
8. Performing Organisation(s) (Name, Address) Forschungszentrum Dresden-Rossendorf e.V. Institut für Sicherheitsforschung Postfach 510119 01314 Dresden	9. Originator's Report No.
	10. Reference No.*) 150 1265
	11a. No. of Pages Report
	11b. No. of Pages Publication
13. Sponsoring Agency (Name, Address) Bundesministeriums für Wirtschaft und Technologie (BMWi) 11019 Berlin	12. No. of References 17
	14. No. of Tables 1
	15. No. of Figures 6
16. Supplementary Notes	
17. Presented at (Title, Place, Date)	

18. Abstract

Turbulence dispersion is a phenomenon of practical importance in many multiphase flow systems. It has a strong effect on the distribution of the dispersed phase. Physically, this phenomenon is a result of interactions between individual particles of the dispersed phase and the continuous phase turbulence eddies. In a Lagrangian simulation, a particle-eddy interaction sub-model can be introduced and the effect of turbulence dispersion is automatically accounted for during particle tracking. Nevertheless, tracking of particle-turbulence interaction is extremely expensive for the small time steps required. For this reason, the Lagrangian method is restricted to small-scale dilute flow problems. In contrast, the Eulerian approach based on the continuum modeling of the dispersed phase is more efficient for densely laden flows. In the Eulerian frame, the effect of turbulence dispersion appears as a turbulent diffusion term in the scalar transport equations and the so-called turbulent dispersion force in the momentum equations. The former vanishes if the Favre (mass-weighted) averaged velocity is adopted for the transport equation system. The latter is actually the total account of the turbulence effect on the interfacial forces. In many cases, only the fluctuating effect of the drag force is important. Therefore, many models available in the literature only consider the drag contribution. A new, more general derivation of the FAD (Favre Averaged Drag) model in the multi-fluid modeling framework is presented and validated in this report.

19. Keywords

Bubbly flow, momentum transfer, bubble forces, turbulent dispersion force, Favre averaging

20. Publisher	21. Price

This report is part of a series, which comprise following reports:

- Construction and execution of experiments at the multi-purpose thermal hydraulic test facility TOPFLOW for generic investigations of two-phase flows and the development and validation of CFD codes (Final project report), FZD-481,
- Experiments on upwards gas-liquid flow in vertical pipes, FZD-482,
- Experiments on two-phase flow in a vertical tube with a moveable obstacle, FZD-483,
- Experimental investigation of stratified air/water flows in a horizontal channel, FZD-484,
- Experimental investigation and CFD simulation of slug flow in horizontal channels, FZD-485,
- CFD models for polydispersed bubbly flows, FZD-486,
- Turbulent Dispersion of Bubbles in Poly-dispersed Gas-Liquid Flows in a Vertical Pipe, FZD-487,
- Validation of the Multiple Velocity Multiple Size Group (CFX10.0 N x M MUSIG) Model for Poly-dispersed Multiphase Flows, FZD-487.

All these reports are published as reports of the Forschungszentrum Dresden-Rossendorf.

Dieser Bericht ist Teil einer Serie, die folgende Einzelberichte umfasst:

- Aufbau und Durchführung von Experimenten an der Mehrzweck-Thermohydraulikversuchsanlage TOPFLOW für generische Untersuchungen von Zweiphasenströmungen und die Weiterentwicklung und Validierung von CFD-Codes (Abschlussbericht), FZD-480,
- Experimente zu aufwärtsgerichteten Gas-Flüssig Strömungen in vertikalen Rohren, FZD-482,
- Experimente zur Zweiphasenströmung in einem vertikalen Rohr mit verschiebbarem Hindernis, FZD-483,
- Experimentelle Untersuchung von geschichteten Luft/Wasser Strömungen in einem horizontalen Kanal, FZD-484,
- Experimentelle Untersuchung und CFD-Simulation von Schwallströmung in horizontalen Kanälen, FZD-485,
- CFD Modelle für polydisperse Blasenströmungen, FZD-486,
- Turbulente Blasendispersion in einer polydispersen Rohrströmung, FZD-487,
- Validierung des N x M MUSIG Modells für polydisperse Mehrphasen-strömungen, FZD-487.

Alle Berichte sind als Berichte des Forschungszentrums Dresden-Rossendorf veröffentlicht.

Contents

1 Introduction

Turbulence dispersion is a phenomenon of practical importance in many multiphase flow systems. It has a strong effect on the distribution of the dispersed phase Especially in bubbly flows in a vertical pipe, turbulent dispersion of bubbles has a strong effect on the radial profile of the gas concentration and its development along the stream. Physically, this phenomenon is a result of interactions between individual particles of the dispersed phase and the continuous phase turbulence eddies. In a Lagrangian simulation, a particle-eddy interaction sub-model can be introduced and the effect of turbulence dispersion is automatically accounted for during particle tracking. Nevertheless, tracking of particle-turbulence interaction is extremely expensive for the small time steps required. For this reason, the Lagrangian method is restricted to small-scale dilute flow problems. In contrast, the Eulerian approach based on the continuum modeling of the dispersed phase is more efficient for densely laden flows. In the Eulerian frame, the effect of turbulence dispersion appears as a turbulent diffusion term in the scalar transport equations and the so-called turbulent dispersion force in the momentum equations. The further vanishes if the Favré (mass-weighted) averaged velocity is adopted for the transport equation system. The latter is actually the total account of the turbulence effect on the interfacial forces. In many cases, only the fluctuating effect of the drag force is important (Loth, 2001; Behzadi et al., 2001). Therefore, many models available in the literature (Gosman et al., 1992; Lopez de Bertodano, 1998; Drew, 2001) only consider the drag contribution except for that of Behzadi et al. (2001). In a recent work (Burns et al., 2004) we developed the FAD (Favré Averaged Drag) model in the multi-fluid modeling framework. Applying the double averaging procedure to the drag force and adopting the Favré averaged velocity, the following expression was obtained for the turbulent dispersion force

$$\mathbf{F}^{p}_{\mathbf{TD}} = -\mathbf{F}^{f}_{\mathbf{TD}} = C\left(\frac{\overline{\alpha^{'}_{f}\mathbf{u}^{'}_{\mathbf{f}}}}{\overline{\alpha_f}} - \frac{\overline{\alpha^{'}_{p}\mathbf{u}^{'}_{\mathbf{f}}}}{\overline{\alpha_p}}\right) \tag{1}$$

where α' and $\mathbf{u}^{'}$ represent the fluctuating component of the volume fraction and the velocity field, respectively. The index f denotes the continuous phase and p the corresponding dispersed phase. We also carried out model validations based on the experimental database of the radial distribution of the gas concentration in fully developed upward gas-liquid flows in a vertical pipe (Prasser et al., 2003).Good agreements were observed between the numerical results and the measurement data (Shi et al., 2004; Frank et al., 2004). Based on the above work, the FAD model has now been implemented as the default model choice in the Eulerian multiphase flow package of the commercial code CFX5.7.

Nevertheless, the physical meaning of the turbulent dispersion force has not been made straightforward in the previous derivation in the Eulerian framework. The validity of the double averaging operation was also not justified. In this work, we provide a new derivation starting from the two-way coupled Lagrangian formulation to overcome these two shortcomings. The derivation not only bridges the two approaches, but also provides a theoretical foundation for applying the FAD model to the Lagrangian solver, which will significantly increase the computational efficiency. Furthermore, the previous validations (Shi et al., 2004; Frank et al., 2004) were limited to mono-disperse bubbly flows with a wall peak of the gas concentration. Here we extend the investigation to

bubbly flows with a core gas peak, in the transition region between wall peak and core peak, and in the finely dispersed flow regime using poly-dispersed models. The intension is to examine the applicability of the FAD model in combination with other interfacial force closures under various complex flow conditions.

2 A new mathematical derivation

For simplicity, the derivation is shown for a mono-dispersed flow with spherical particles. Here and in the following text the term *particle* is referred to as a single unit of the dispersed phase including solid particles, droplets or bubbles, while the term *fluid* to the continuous carrier phase. The following formulation can be applied to Lagrangian particle tracking,

$$\mathbf{x_p}^{n+1} = \mathbf{x_p}^{n} + \mathbf{V_p}^{n}\delta t \tag{2}$$

$$\begin{aligned}\frac{\mathbf{V_p}^{n+1} - \mathbf{V_p}^{n}}{\delta t} = & \left(\frac{3}{4}\frac{\rho_f}{\rho_p}\frac{C_D}{d_p}|\mathbf{V_p} - \mathbf{V_f}|\right)^{n} (\mathbf{V_p}^{n+1} - \mathbf{V_f}^{n+1}) \\ & + \frac{1}{\rho_p \delta V}\mathbf{F_{other}}\end{aligned} \tag{3}$$

where $\mathbf{x_p}$ and $\mathbf{V_p}$ respectively denote the position and the velocity of the particle, δ_t the length of the time step, and n, $n+1$ the index of the time step. The first term on the right hand side of eq. (3) corresponds to the drag force per unit particle mass. The other forces are included in $\mathbf{F_{other}}$. Other quantities are, ρ_f and ρ_p material density of the continuum and disperse, respectively, C_D the drag coefficient, d_p and δV the diameter and volume of the particle, and $\mathbf{V_f}$ the fluid velocity experienced by the particle. Except for in a DNS, this velocity needs to be constructed based on the velocity field $\mathbf{U_f}$ obtained in the Eulerian frame and a fluctuating component $\mathbf{v_f}$ from a particle-eddy interaction (statistic) model, namely

$$\mathbf{V_f}^{n+1} = \overline{\mathbf{U_f}(\mathbf{x_p}^{n+1}, t)} + \mathbf{v_f}^{n+1} \tag{4}$$

2.1 Ensemble Average in the Eulerian-Lagrangian Frame

The instant local interfacial momentum exchange can be calculated from the ensemble average of the interfacial forces over each computational grid cell. Considering a computational grid cell with a volume $\triangle V$ which encloses or intersects $n(t_j)$ particles at a time instant t_j of the Lagrangian calculation and assuming that only the drag contribution is essential, the momentum source per unit volume on the carrier phase is

$$\mathbf{F_D}(t_j) = \frac{1}{\triangle V}\sum_{i=1}^{n(t_j)} \frac{3}{4}\rho_f \frac{C_D^i}{d_p}|\mathbf{V_p^i} - \mathbf{V_f^i}|(\mathbf{V_p^i} - \mathbf{V_f^i})\delta V \tag{5}$$

In order to express eq. (10) in terms of the Eulerian variables, we introduce Favre (mass-weighted) averaged variables for the particle ensemble,

$$\Phi(t_j) = \frac{\sum_{i=1}^{n(t_j)} \rho_p \, \Phi^i \delta \, V}{\sum_{i=1}^{n(t_j)} \rho_p \, \delta V} = \frac{1}{\triangle V}\frac{\sum_{i=1}^{n(t_j)} \Phi^i \delta V}{\alpha_p(t_j)} \tag{6}$$

where Φ^i represents the Lagrangian quantity related to the i-th particle while $\Phi(t_j)$ is a field variable resulting from the ensemble average, and α_p is the volume fraction of the dispersed phase defined as

$$\alpha_p(t_j) = \frac{1}{\triangle V} \sum_{i=1}^{n(t_j)} \delta V = \frac{n(t_j)\,\delta V}{\triangle V} \tag{7}$$

Introducing $\mathbf{U_p}$ to represent the particle velocity field and utilizing eq. (4), eq. (5) can be formulated as follows,

$$\begin{gathered} \mathbf{F_D}(t_j) = \alpha_p(t_j)\mathbf{f_D}(t_j) \text{ , where} \\ \mathbf{f_D}(t_j) = \frac{3}{4}\rho_f \frac{C_D}{d_p}|\mathbf{U_p} - \mathbf{U_f}|(\mathbf{U_p} - \mathbf{U_f}) \end{gathered} \tag{8}$$

where the drag coefficient C_D is a field variable in the sense of statistics.

2.2 Reynolds Averaging in the Eulerian Frame

The particle-eddy interaction model requires the Lagrangian time step δt to be much smaller than the characteristic turbulence eddy life time, τ_e, and the time for a particle to travel over the mean eddy length (ℓ_e), $\tau_i = \ell_e/|\mathbf{U_p} - \mathbf{U_f}|$. For isotropic turbulent flow, τ_e, ℓ_e and the turbulence velocity scale u_e can be estimated as follows

$$\tau_e = \frac{\ell_e}{u_e} = C_L \frac{k_f}{\epsilon_f}, \quad \ell_e = C_\mu^{3/4} \frac{k_f^{3/2}}{\epsilon_f}, \quad u_e = \sqrt{\frac{2k_f}{3}} \tag{9}$$

where k_f is the fluid turbulence kinetic energy and ϵ_f the corresponding dissipation rate. $C_\mu \approx 0.09$ is an empirical constant, which results in $C_L \approx 0.20$. Nevertheless, different empirical values were reported or applied in the literature, e.g, 0.27 in Loth (2001) or about 0.41 in Gosman et al. (1992).

On the other hand, the Eulerian time step is usually larger than τ_e and τ_i, and consists of a number of Lagrangian time steps, say $T_E = 2N\,\delta t$. Therefore, the momentum source for the Eulerian calculation is equal to the Reynold average of eq. (5) over T_E,

$$\overline{\mathbf{F_D}} = \frac{1}{\triangle V}\frac{1}{T_E} \sum_{j=-N}^{N} \sum_{i=1}^{n(t_j)} \frac{3}{4}\rho_f \frac{C_D^i}{d_p}|\mathbf{V_p^i} - \mathbf{V_f^i}|(\mathbf{V_p^i} - \mathbf{V_f^i})\delta V \delta t \tag{10}$$

2.3 The Turbulent Dispersion Force Model

With reference to eq. (8), we could express the Reynolds averaged drag force (10) as follows

$$\overline{\mathbf{F_D}} = \overline{\alpha_p}\,\overline{\mathbf{f_D}} + \overline{\alpha_p' \mathbf{f_D'}} \tag{11}$$

where $\mathbf{f_D'}$ is the fluctuating component of $\mathbf{f_D}$ given in eq. (8) and α_p' the fluctuating component of α_p. Thereby, we obtain a mean drag force term $\overline{\alpha_p}\,\overline{\mathbf{f_D}}$ and a turbulent dispersion force term $\overline{\alpha_p' \mathbf{f_D'}}$ in terms of the Reynolds averaged variables.

In order to simplify the the multi-fluid model equations it is advantageous to adopt the Favré averaged velocity as defined below

$$\tilde{\mathbf{U}}_{\mathbf{k}} = \frac{\overline{\rho_k \alpha_k \mathbf{U}_{\mathbf{k}}}}{\overline{\rho_k \alpha_k}} = \overline{\mathbf{U}_{\mathbf{k}}} + \frac{\overline{\alpha_k^{'} \mathbf{u}_{\mathbf{k}}^{'}}}{\overline{\alpha_k}} \tag{12}$$

, where k is the phase indicator. Decomposing the instant velocity into various mean and fluctuating components

$$\mathbf{U}_{\mathbf{k}} = \tilde{\mathbf{U}}_{\mathbf{k}} + \mathbf{u}_{\mathbf{k}}^{''} = \overline{\mathbf{U}}_{\mathbf{k}} + \mathbf{u}_{\mathbf{k}}^{'} \tag{13}$$

we have the following relationships

$$\tilde{\mathbf{U}}_{\mathbf{k}} = \overline{\mathbf{U}}_{\mathbf{k}} - \overline{\mathbf{u}_{\mathbf{k}}^{''}}, \quad \mathbf{u}_{\mathbf{k}}^{''} = \mathbf{u}_{\mathbf{k}}^{'} - \overline{\mathbf{u}_{\mathbf{k}}^{''}}, \quad \overline{\mathbf{u}_{\mathbf{k}}^{''}} = -\frac{\overline{\alpha_k^{'} \mathbf{u}_{\mathbf{k}}^{'}}}{\overline{\alpha_k}} \tag{14}$$

Obviously, $\overline{\alpha_k^{'} \mathbf{u}_{\mathbf{k}}^{''}} = 0$. That leads to a continuity equation without a turbulent diffusion term,

$$\frac{\partial}{\partial t}(\rho_k \overline{\alpha}_k) + \nabla \cdot (\rho_k \overline{\alpha}_k \tilde{\mathbf{U}}_{\mathbf{k}}) = 0 \tag{15}$$

Applying eqs. (13) and (14) to eq. (11), we can obtain the mean drag in terms of the Favré averaged velocities and the turbulent dispersion force

$$\begin{aligned} \overline{\mathbf{F_D}} \approx & \underbrace{\frac{3}{4}\rho_f \frac{\overline{C_D}}{\overline{d_p}}}_{D} \overline{|\left(\mathbf{U_p} - \mathbf{U_f}\right)|} \, \overline{\alpha_p \left(\mathbf{U_p} - \mathbf{U_f}\right)} \\ = & \underbrace{D\overline{\alpha_p}\overline{|\mathbf{U_p} - \mathbf{U_f}|} \left(\tilde{\mathbf{U}}_{\mathbf{p}} - \tilde{\mathbf{U}}_{\mathbf{f}}\right)}_{\text{mean drag}} \\ & + \underbrace{D\overline{|\mathbf{U_p} - \mathbf{U_f}|} \left(\frac{\overline{\alpha_p}}{\overline{\alpha_f}} \overline{\alpha_f^{'} \mathbf{u}_{\mathbf{f}}^{'}} - \overline{\alpha_p^{'} \mathbf{u}_{\mathbf{f}}^{'}}\right)}_{\text{turbulent dispersion force } \mathbf{F_{TD}^f}} \end{aligned} \tag{16}$$

It is assumed that $\overline{|\mathbf{U_p} - \mathbf{U_f}|} \approx |\tilde{\mathbf{U}}_{\mathbf{p}} - \tilde{\mathbf{U}}_{\mathbf{f}}|$ in Burns et al. (2004). A more accurate evaluation can be made as follows. Assume that

$$\overline{|\mathbf{U_p} - \mathbf{U_f}|} \approx \left[\overline{\mathbf{U}}_{\mathbf{r}} \cdot \overline{\mathbf{U}}_{\mathbf{r}} + \overline{\mathbf{u}_{\mathbf{r}}^{'} \cdot \mathbf{u}_{\mathbf{r}}^{'}}\right]^{1/2} \tag{17}$$

where $\phi_{\mathbf{r}}$ denotes $\phi_{\mathbf{p}} - \phi_{\mathbf{f}}$, $\overline{\mathbf{U}}_{\mathbf{r}} \cdot \overline{\mathbf{U}}_{\mathbf{r}}$ can be expressed as

$$\overline{\mathbf{U}}_{\mathbf{r}} \cdot \overline{\mathbf{U}}_{\mathbf{r}} = \tilde{\mathbf{U}}_{\mathbf{r}} \cdot \tilde{\mathbf{U}}_{\mathbf{r}} + (\overline{\mathbf{u}_{\mathbf{p}}^{''}} - \overline{\mathbf{u}_{\mathbf{f}}^{''}}) \cdot \left[(\overline{\mathbf{u}_{\mathbf{p}}^{''}} - \overline{\mathbf{u}_{\mathbf{f}}^{''}}) - 2\tilde{\mathbf{U}}_{\mathbf{r}}\right] \tag{18}$$

The particle fluctuating velocity $\mathbf{u}_{\mathbf{p}}^{'}$ can be related to the fluid counterpart by the following expression

$$\mathbf{u}_{\mathbf{p}}^{'} = \mathbf{u}_{\mathbf{f}}^{'} \left(1 - e^{-1/St}\right) \tag{19}$$

where St is the Stokes number defined as the ratio of the particle response time τ_p to the eddy life time τ_e,

$$St = \tau_p/\tau_e \ , \qquad \tau_p = \frac{4}{3}\frac{\rho_p}{\rho_f}\frac{d_p}{C_D\,|\mathbf{U_p} - \mathbf{U_f}|} \tag{20}$$

Then, we have

$$\mathbf{u_r}^{'} = -\mathbf{u_f}^{'} e^{-1/St}, \qquad \overline{\mathbf{u_p}^{''}} = -\frac{\overline{\alpha_p^{'}\mathbf{u_f}^{'}}}{\overline{\alpha_p}}\left(1 - e^{-1/St}\right) \tag{21}$$

In addition, we have $\overline{\mathbf{u_r}^{'} \cdot \mathbf{u_r}^{'}} = 2k_f e^{-2/St}$, where $k_f = 1/2\overline{\mathbf{u_f}^{'} \cdot \mathbf{u_f}^{'}}$ is the turbulent kinetic energy of the fluid. Adopting the eddy diffusivity hypothesis (EDH),

$$\overline{\alpha_k^{'}\mathbf{u_f}^{'}} = -\frac{\nu_{f,t}}{\sigma_k}\nabla\overline{\alpha}_k \tag{22}$$

where σ_k is the turbulent Schmidt number of phase k to be determined empirically and reported to be 0.72 for air-water flow (Moraga et al., 2003), we have

$$\overline{\mathbf{u_f}^{''}} = \frac{\nu_{f,t}}{\sigma_f\,\overline{\alpha}_f}\nabla\overline{\alpha_f}, \quad \overline{\mathbf{u_p}^{''}} = \frac{\nu_{f,t}}{\sigma_p\,\overline{\alpha_p}}\nabla\overline{\alpha_p}\left(1 - e^{-1/St}\right) \tag{23}$$

With reference the above expressions, the turbulent dispersion force on the dispersed phase, which is opposite to the force on the fluid $\mathbf{F_{TD}^f}$, can be expressed as follows

$$\mathbf{F_{TD}^p} \approx -\frac{\nu_{f,t}}{\overline{\alpha_f}}\overline{C_D|\mathbf{U_p} - \mathbf{U_f}|}\left(\frac{\overline{\alpha_f}}{\sigma_p}\nabla\overline{\alpha_p} - \frac{\overline{\alpha_p}}{\sigma_f}\nabla\overline{\alpha_f}\right) \tag{24}$$

In the case of the two-fluid model, one has $\overline{\alpha_p} + \overline{\alpha_f} = 1$ and $\sigma_p = \sigma_f$. Therefore

$$\mathbf{F_{TD}^p} \approx -\frac{3}{4}\rho_f\frac{\overline{C_D}}{\overline{d_p}}\frac{\nu_{f,t}}{\sigma_f\,\overline{\alpha_f}}\overline{|\mathbf{U_p} - \mathbf{U_f}|}\nabla\overline{\alpha_p} \tag{25}$$

Equations (24) and (25) are equivalent to the model formulations in Burns et al. (2004) and several other models in the literature (Gosman et al., 1992; Lopez de Bertodano, 1998; Drew, 2001), in the limit of dilute flow of spherical particles. Hence we have derived the FAD model from a new way. Moreover, considering its starting point this derivation has also provided a theoretical foundation for applying the FAD model to the Lagrangian solver, which is expected to increase the computational efficiency significantly.

3 Validation and evaluation

Model validations is based on numerical and experimental investigations of upward bubbly flows in a vertical pipe. The numerical results are compared with the experimental data for the radial distribution of the gas concentration measured in the fully developed flow region. Details are described below.

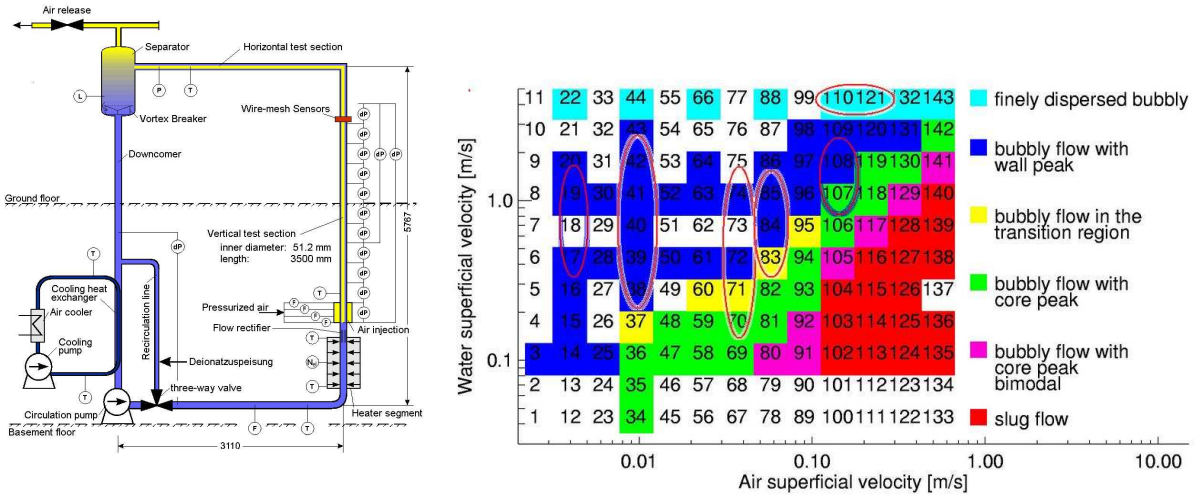

Fig. 3.1: MTLoop test facility (left) and the selected test cases (right).

3.1 Experimental Set Up and Test Case Definitions

The experiments were carried out on the MTLoop test facility of FZR illustrated in Fig. 3.1 (above). The test section is 4 m long and has an inner diameter $D = 51.2$ mm. The Loop was operated under atmospheric pressure and a constant temperature of 30 °C. Measurements were carried out for stationary flows of various air-water superficial velocity ratios at 10 different cross sections located between $L/D = 0.6$ and 59.2 from the gas injection using a wire-mesh sensor with 24×24 electrodes. Careful measures were taken to ensure axial-symmetry of the macroscopic flow. Details are described in Prasser et al. (2003). The test cases defined are marked in Fig. 3.1 (below). They covers bubbly flows with a wall, core gas peak, in the transition region between them, and finely dispersed flows. The cases where the mono-dispersed flow assumption applies have been reported in Shi et al. (2004); Frank et al. (2004). Here we present some results for poly-dispersed flows. The experimental data measured at $L/D = 59.2$ were chosen for the validation, where the flow is fully developed and the gas concentration profile is independent of the inlet condition (Shi et al., 2004).

3.2 Numerical Settings

The numerical simulation was based on the CFX multi-fluid model using the User-Fortran implementation of the FAD model in the commercial CFD package CFX-5.6 (Shi et al., 2004) and also the formally released implementation in CFX-5.7. Both the liquid and the gas phase were assumed to be incompressible. Adopting the eddy viscosity hypothesis, the Reynolds averaged governing equations for mass and momentum transport can be written as follows:

$$\frac{\partial}{\partial t}(\alpha_k \rho_k) + \nabla \cdot (\alpha_k \rho_k \mathbf{U}_k) = 0 \tag{26}$$

$$\frac{\partial}{\partial t}(\alpha_k \rho_k \mathbf{U}_k) + \nabla \cdot (\alpha_k \rho_k \mathbf{U}_k \mathbf{U}_k) = -\alpha_k \nabla P - \nabla \cdot \left[\alpha_k \mu_{k,eff} \left(\nabla \mathbf{U}_k + \nabla^{\mathbf{T}} \mathbf{U}_k\right)\right] + \alpha_k \rho_k \mathbf{g}_k + \mathbf{M}_k \tag{27}$$

where k is the phase indicator, α the volume fraction, $\mathbf{U}$ the velocity, P the pressure shared by both phases, $\mu_{k,eff}$ the effective dynamic viscosity consisting of the material (μ_k) and turbulence eddy ($\mu_{k,t}$) contributions, $\mathbf{g}$ the gravity acceleration, and $\mathbf{M}$ the interfacial forces including the drag ($\mathbf{F_D}$), lift ($\mathbf{F_L}$), wall foce ($\mathbf{F_W}$) and turbulence dispersion force ($\mathbf{F_{TD}}$). The following models were appied for the interfacial forces: the Grace model (Grace and Weber, 1982) for the drag force, the Tomiyama correlation for the lift and wall lubrication force (Tomiyama et al., 1995; Tomiyama, 1998), and the FAD model for the turbulence dispersion force. The Tomiyama lift force model is as follows:

$$\mathbf{F}_\mathbf{L}^g = -C_L \alpha_g \rho_\ell (\mathbf{U}_g - \mathbf{U}_\ell) \times \nabla \times \mathbf{U}_\ell \tag{28}$$

where C_L is the lift coefficient defined by

$$C_L = \begin{cases} \min[0.288 \tanh(0.121 Re_p), f(Eo_d)], & Eo_d < 4 \\ f(Eo_d) = 0.00105 Eo_d^3 - 0.0159 Eo_d^2 - 0.0204 Eo_d + 0.474, & 4 \le Eo_d \le 10.7 \\ -0.29, & Eo_d > 10.7 \end{cases} \tag{29}$$

Here Eo_d is the Eötvös number based on the long axis d_H of a deformable bubble, i.e.

$$Eo_d = \frac{(\rho_\ell - \rho_g)\, g_{eff}\, d_H^2}{\sigma}, \text{ with } d_H = d_p(1 + 0.163 Eo^{0.757})^{1/3} \text{ and } Eo = \frac{(\rho_\ell - \rho_g)\, g_{eff}\, d_p^2}{\sigma} \tag{30}$$

And the wall force model by Tomiyama (1998) is

$$\mathbf{F}_\mathbf{W}^g = -C_W \alpha_g \rho_\ell |\mathbf{U_r} - (\mathbf{U_r} \cdot \mathbf{n_w})\mathbf{n_w}|^2 \frac{d_p}{2} \left[\frac{1}{y_w^2} - \frac{1}{(D - y_w)^2} \right] \mathbf{n_w} \tag{31}$$

with a coefficient as a function of the Eötvös number,

$$C_W = \begin{cases} \exp(-0.933 Eo + 0.179) & \text{if } 1 \le Eo \le 5, \\ \min(0.0059905 Eo - 0.0186865, 0.179) & \text{if } Eo > 5 \end{cases} \tag{32}$$

The added mass force was neglected for the stationary fully developed flow considered here. Detailed validation of the above non-drag force models for mono-dispersed bubbly flows has been reported by Shi et al. (2004).

The bubbles were classified into several size classes and each was treated as a continuum fluid. According to eq. (29), the lift force on a bubble changes the sign when the Eötvös number Eo exceeds a critical value about 10.7 for the current air-water system under atmospheric pressure and the ambient temperature, corresponding to a critical diameter about 5.8 mm. Hence bubbles over this critical size were separated from those smaller. The computational input are specified in Table 3.1. In a previous work (Shi et al., 2004), we found the $k - \omega$ based Shear Stress Transport (SST) turbulence model (Menter, 1994) to yield superior predictions to the $k - \varepsilon$ model. Hence the SST model was applied to the liquid phase turbulence in the present study. Particle induced turbulence was accounted for by using the enhanced eddy viscosity model of Sato and Sekoguchi (1975) and Sato et al. (1981), which which adds a bubble induced eddy viscosity to the fluid phase turbulence

$$\mu_{t,b} = C_\mu \alpha_g \rho_\ell d_p |\mathbf{U}_g - \mathbf{U}_\ell| \tag{33}$$

Tab. 3.1: Test case definitions, U_ℓ, U_g–superficial velocity, d_p–diameter [mm], VF–gas volume fraction.

Index	U_ℓ	U_g	Air	Air 1		Air 2		Air 3	
	[m/s]	[m/s]	VF[%]	d_p	VF[%]	d_p	VF[%]	d_p	VF[%]
070	0.161	0.0368	22.86	4.8	12.20	7.0	10.66		
071	0.255	0.0368	14.43	4.8	11.27	6.6	3.16		
083	0.405	0.0574	12.76	3.7	1.00	5.0	8.86	6.7	2.90
084	0.641	0.0574	8.95	4.6	8.24	6.4	0.71		
107	1.017	0.140	13.77	5.1	9.47	6.8	4.30		
110	4.047	0.140	3.46	2.4	1.71	3.4	1.75		

The dispersed phase turbulence was treated by an algebraic model assuming the kinematic eddy viscosity to be proportional to the value of the continuous phase, i.e. $\nu_{t,p} = \nu_{t,f}/\sigma_p$. Here and also in the FAD model the turbulent Schmidt number σ_k was set equal to unity for each phase.

A computational domain consisting of a 60 degree sector of the pipe with the symmetry condition on both sector faces was applied in the simulation. A uniform volume fraction distribution was assumed for both phases at the inlet together with a $1/7$-th power inlet velocity profile $U_{in} = 1.224U_0\,(1 - r^*)^{1/7}$, where U_0 is the mean velocity and $r^* = 2r/D$ the dimensionless radial coordinate. The radial velocity was assumed to be null. In addition, a medium turbulence intensity (5%) was assigned there. The outlet was located at 3.3 m away from the inlet, where an averaged static pressure equal to the atmospheric pressure P_0 was assigned. No-slip condition together with the CFX5 build-in wall functions for the turbulence models was applied for the liquid at the wall, whereas a free-slip wall condition was assumed for the gas. The pressure field was initialized using the expression $P = P_0 + \rho_\ell|\mathbf{g}|(3.3 - L)$. The convergence error, grid dependence of the numerical results and the inlet condition effect were carefully examined. Details were reported in Shi et al. (2004).

3.3 Results and Discussion

Some results for bubbly flows with low gas superficial velocities ($U_g < 0.06$ [m/s]) are presented in Fig. 3.2. The computational results for the radial profile of the air volume fraction at the cross section chosen for validation are compared with the corresponding measurement data. The numerical results for each dispersed phase are also plotted for reference. The volume fraction is normalized by the mean value over the cross section as defined below.

$$\alpha_g^* = \frac{\alpha_g}{\alpha_{g,0}}, \text{ with } \alpha_{g,0} = 2\int_0^1 \alpha_g(r^*)\; r^* \mathrm{d}r^* \tag{34}$$

These cases cover a wide range of complex flow conditions, namely with a core gas peak (070), a wall gas peak (084), and in transition region (071, 083). Good agreements between computation and measurement can be observed. Similar trends are observed for the other test cases with a wall gas peak (not shown here). This confirms the applicability of the FAD turbulent dispersion force model in combination with the other non-drag force models to bubbly flows under these conditions. In addition, due

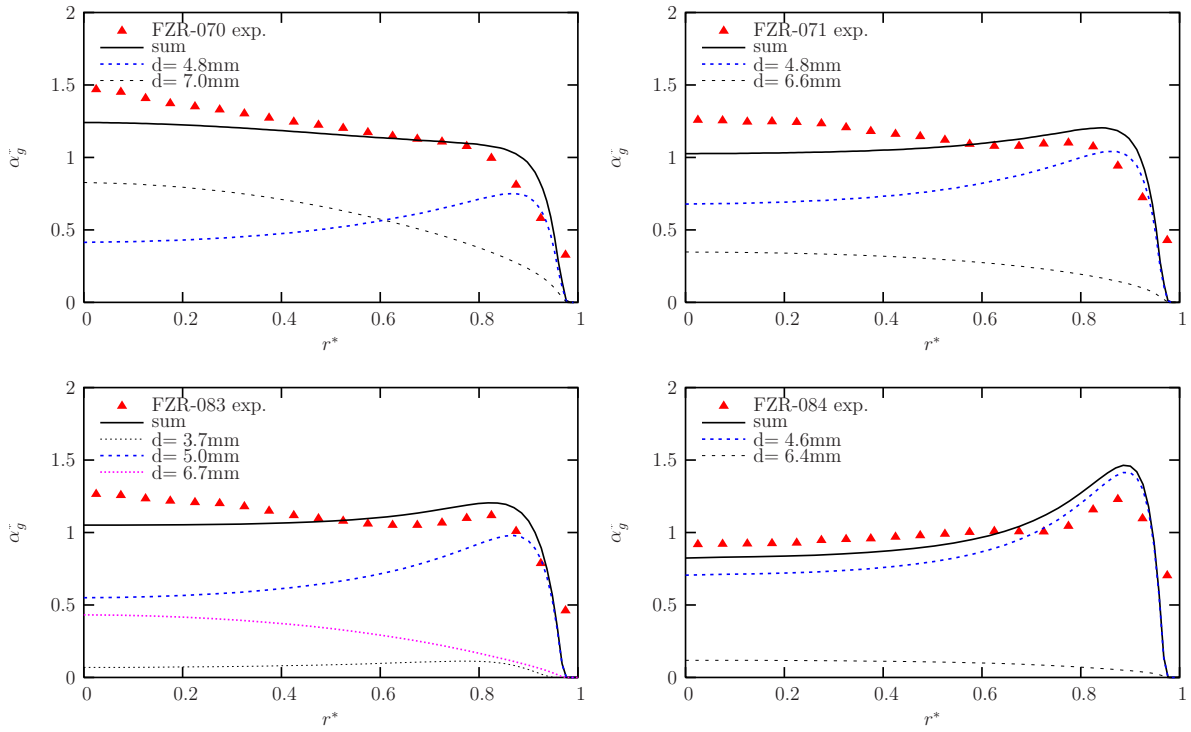

Fig. 3.2: Comparison of the numerical results and measurement data for the radial profile of the gas volume fraction at $L/D = 59.2$.

to the Tomiyama lift force model (Tomiyama, 1998), a core gas peak was predicted for the dispersed phase with a bubble diameter larger than 5.8 mm and a wall peak for the smaller bubbles. This is consistent with experimental observations.

It is interesting to examine the behavior of various non-drag forces. The radial distributions of these forces from the computation are displayed in Fig. 3.3 for both dispersed phases of the case 070. The results show that the wall force is limited to the near-wall region. Due to the high gradient in the volume fraction of Air1 occurring in the wall peak region, the turbulent dispersion force there has a high magnitude and is the important force component to balance the wall force. Beyond the wall proximity, the balance between the lift and the turbulent dispersion force determines the radial distribution of the gas volume fraction in a fully developed flow.

In Fig. 3.4 we also present two examples where agreements between computation

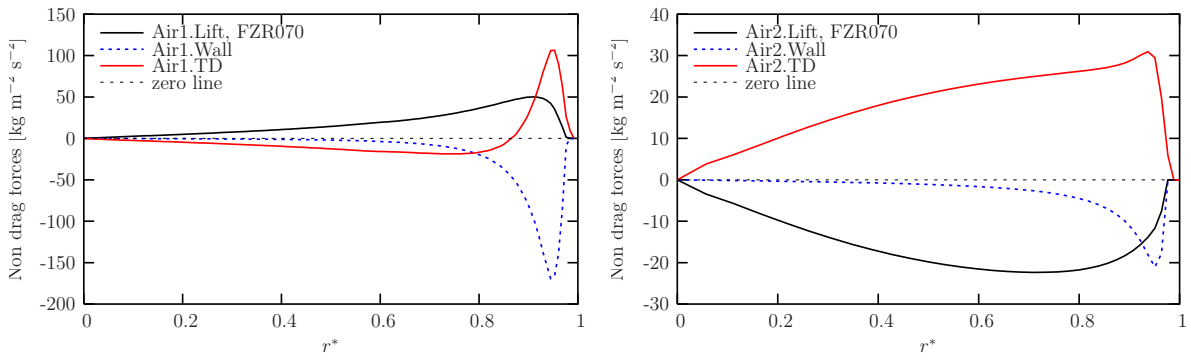

Fig. 3.3: Radial distribution of non-drag forces, FZR070.

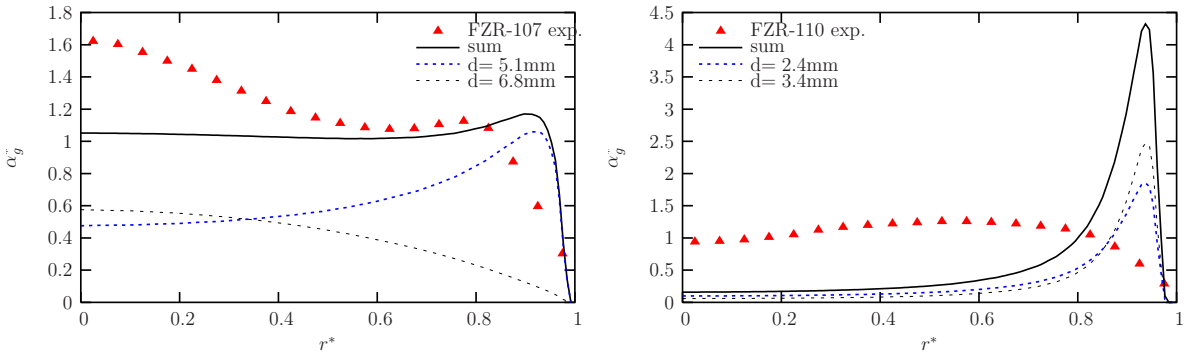

Fig. 3.4: Two examples of unsatisfactory agreements between computation and measurements; radial distribution of the gas volume fraction at $L/D = 59.2$.

and measurements are unsatisfactory, namely 107 (transition region) with a larger gas superficial velocity $U_g = 0.140$ [m/s], and 110 (finely dispersed flow). Considering that the turbulent dispersion force model is the only one among the non-drag force models being physically well founded and mathematically rigorously derived, the problem should be due to the lift or wall force model. They seem to cease to be valid under these flow conditions. In the present work, we focus on the turbulent dispersion force model and leave the uncertainties in the other non-drag forces to be clarified in the future investigation.

With reference to eqs. (24) and (25), the turbulent dispersion force is a function of the drag coefficient C_D and the slip velocity $|\tilde{\mathbf{U}}_\mathbf{p} - \tilde{\mathbf{U}}_\mathbf{f}|$, which again depends on C_D. Hence it is important to examine the influence of the drag closure model on the numerical results. For that purpose, some calculations were repeated by applying the drag model of Ishii and Zuber (1979). The comparison of the corresponding results with those obtained based on the Grace model (Grace and Weber, 1982) are displayed in Fig. 3.5 for the test case 070 and in Fig. 3.6 for the case 110, respectively. In case 070, some small differences in the drag coefficient C_D and in the slip velocity were predicted due to different drag models. Consequently, the same trend can be expected for the turbulent dispersion force. This is shown by the results for the turbulent dispersion force coefficient C_{TD}. The definition (35) is based on eq. (24), namely under the two-fluid model assumption. However, this is a good approximation to the true value and is suitable for the evaluation.

$$C_{TD} \approx \frac{3}{4}\rho_f \frac{C_D}{d_p}\frac{\nu_{f,t}}{\sigma_f}\,|\tilde{\mathbf{U}}_\mathbf{p} - \tilde{\mathbf{U}}_\mathbf{f}|, \tag{35}$$

The differences in the volume fraction are discernible for each bubble group, but is insignificant. In the latter case (110), the results almost show no drag model effect. Hence, these results allow us to conclude that the influence of the drag model on the turbulence dispersion and on the numerical results is insignificant. In addition, it is interesting to note the larger slip velocities observed for the smaller bubbles in the case 110 ($d_p = 2.4$, 3.4mm) than for those larger ones in the case 070 ($d_p = 4.8$, 7.0mm). These results are self consistent considering the lower C_D obtained for the smaller bubbles in the case 110. This observation acn be understood with reference to Grace and Weber (1982) for a diagram of the terminal velocity as a function of the bubble diameter, which indicates a local velocity peak at $d_p \approx 2$ mm for ellipsoidal air bubbles in pure water as in the present study. The results also show that the turbulence

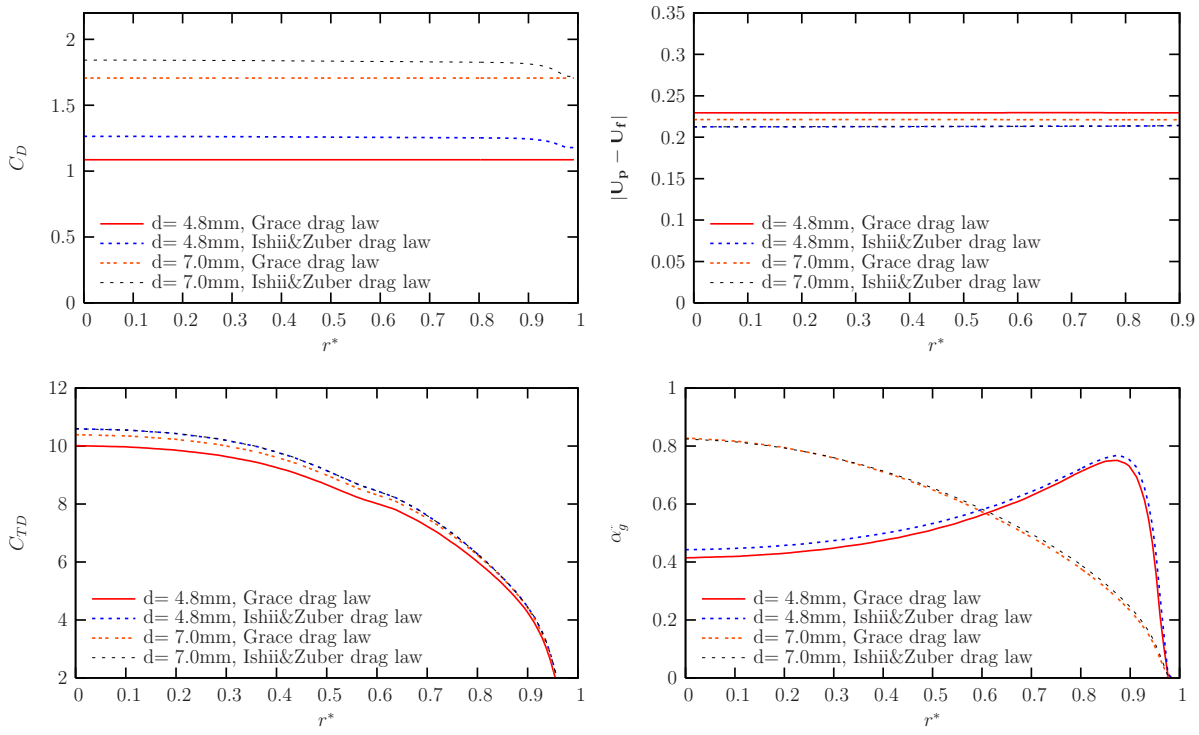

Fig. 3.5: Radial profile of the drag coefficient C_D, the slip velocity $|\tilde{\mathbf{U}}_\mathbf{p} - \tilde{\mathbf{U}}_\mathbf{f}|$, the turbulent dispersion force coefficient C_{TD} and the volume fractions α_g^* based on different drag models (Grace and Weber, 1982; Ishii and Zuber, 1979), FZR070.

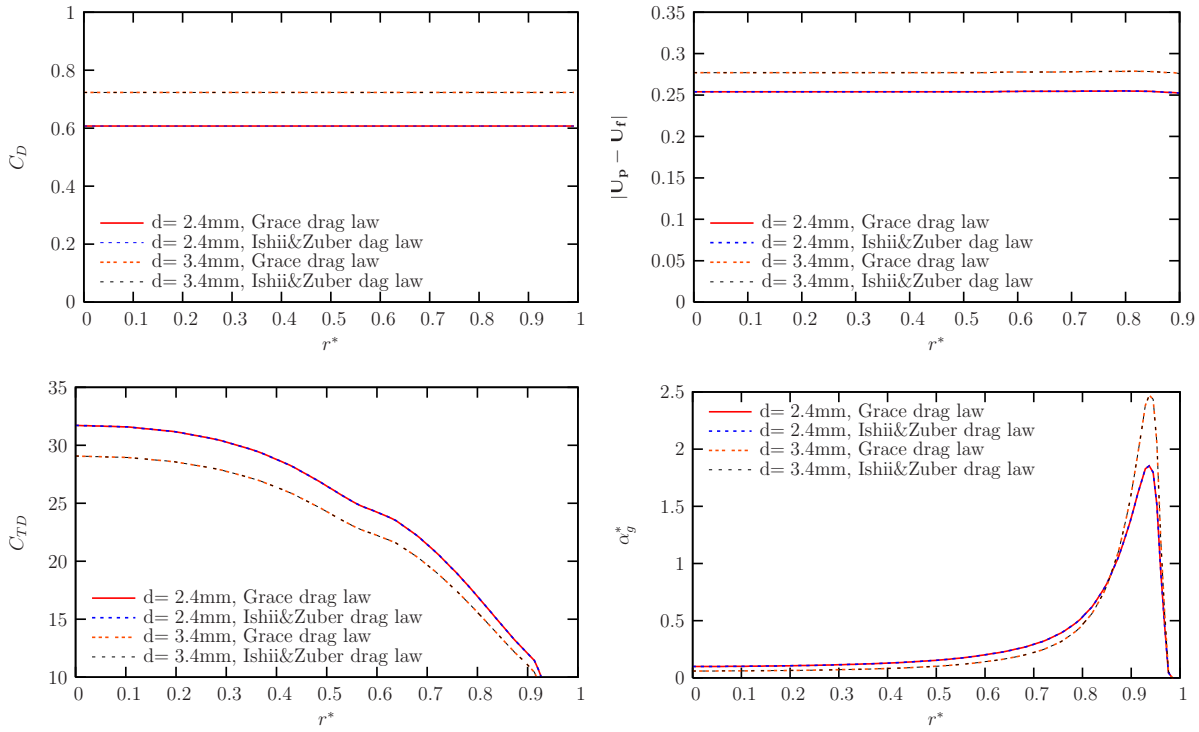

Fig. 3.6: Radial profile of the drag coefficient C_D, the slip velocity $|\tilde{\mathbf{U}}_\mathbf{p} - \tilde{\mathbf{U}}_\mathbf{f}|$, the turbulent dispersion force coefficient C_{TD} and the volume fractions α_g^* based on different drag models (Grace and Weber, 1982; Ishii and Zuber, 1979), FZR110.

dispersion is much stronger in the case 110. This is due to the higher turbulent eddy viscosity $\nu_{f,t}$ corresponding to the higher Reynolds number of the liquid flow in this case. Also, the bubble diameter is much smaller in the finely dispersed flow regime.

4 Conclusion

A new mathematical derivation is presented for the turbulent dispersion force model for Eulerian multiphase flows. We started from the Lagrangian approach and explained the physics in a straightforward way. This derivation also provides a theoretical foundation for applying this model to the Lagrangian solver, which will significantly increase the computational efficiency. Furthermore, we have carried out extensive model evaluations by numerical and experimental investigations of bubbly flows in a vertical pipe under various flow conditions. Poly-dispersed models were applied in the computations. The results indicate that the FAD model in combination of other interfacial force models applied in the numerical simulation is applicable to bubbly flows both with a wall and a core gas peak and to flows in the transition region with a low gas superficial velocity. Unsatisfactory agreements between simulation and measurements were observed in the finely dispersed flow regime and in the transition region with a high gas superficial velocity. Nevertheless, it seems that this is due to the uncertainties in the lift and wall force models. The results also show that the bubble size and the liquid flow Reynolds number have a strong effect on the turbulent dispersion, as is indicated in the model derivation. The influence of the drag law on the turbulent dispersion force and also on the numerical results was found to be insignificant.

References

Behzadi, A. et al. (2001). In ICMF 2001, 4th Int. Conf. on Multiphase Flow, New Orleans, LA, USA.

Burns, A. et al. (2004). In ICMF 2004, 5th Int. Conf. on Multiphase Flow, Paper No.392, Yokohama, Japan.

Drew, D.A. (2001). J Eng. Math., Vol.41, pp 259–274.

Frank, T. et al. (2004). In 3rd Int. Symposium on Two-Phase Flow Modelling and Experimentation, pages 1–8, Pisa, Italy.

Gosman, A.D. et al. (1992). AIChE J, Vol.38, pp. 1946–1956.

Grace, J. R. and Weber, M. E. (1982). Handbook of Multiphase Systems, chapter Hydrodynamics of drops and bubbles. Hemisphere.

Ishii, M. and Zuber, N. (1979). AIChE J., Vol. 25, pp. 843–855.

Lopez de Bertodano, A. (1998). Nuclear Engng. Design, Vol. 179, pp. 65–74.

Loth, E. (2001). Int. J. Multiphase Flow, Vol. 27, pp. 1051–1063.

Menter, F.R. (1994). AIAA-Journal, Vol. 32.

Moraga, F.J. et al. (2003). Int. J. Multiphase Flow, Vol. 29, pp. 655–673.

Prasser, H.-M. et al. (2003). Technical Report FZR-379, Forschungszentrum Rossendorf.

Sato, Y. et al. (1981). Int J Multiphase Flow, Vol. 7, pp. 167–178.

Sato, Y. and Sekoguchi, K. (1975). Int. J. Multiphase Flow, Vol. 2 pp. 79.

Shi, J.-M., et al. (2004). In ICMF 2004, 5th Int. Conf. Multiphase Flow, Paper No.392, Yokohama, Japan.

Tomiyama., A. (1998). In ICMF 98, 3rd Int. Conf. Multiphase Flow, Lyon, France.

Tomiyama, A., et al. (1995). In Serizawa, A., et al., editors, Advances in Multiphase Flow, pp. 3–15. Elsevier Science.

List of Figures

List of Tables